Evidence for Tilted Smectic Liquid Crystalline Packing of fd *Inovirus* from X-ray Fiber Diffraction

L. C. Welsh,[†] M. F. Symmons,[‡] C. Nave,[§] R. N. Perham,[‡] E. A. Marseglia,[†] and D. A. Marvin*[,‡]

Cavendish Laboratory, University of Cambridge, Madingley Road, Cambridge, CB3 OHE, U.K., Cambridge Centre for Molecular Recognition, Department of Biochemistry, University of Cambridge, Tennis Court Road, Cambridge, CB2 1QW, U.K., and CLRC Daresbury Laboratory, Warrington, WA4 4AD, U.K.

Received April 16, 1996; Revised Manuscript Received July 29, 1996[⊗]

ABSTRACT: Fibers of the fd strain of *Inovirus* (filamentous bacteriophage) prepared above its isoelectric point (about pH 4) give X-ray diffraction patterns, "higher pH patterns", that differ from the patterns of fd fibers below the isoelectric point, "lower pH patterns". The overall distribution of intensity on higher and lower pH patterns is substantially the same, indicating that the virion structure is substantially the same, but the crystalline reflections that define the packing of the virions in crystallites are different. For the lower pH patterns, the crystalline reflections can be indexed on a conventional hexagonal lattice. However, for the higher pH patterns, the crystalline reflections on the equator and first layer line are spread out in a broad, angular, but specific fashion ("layer-line fanning"), unlike disorientation spreading. We interpret this observation to mean that the crystallites in the higher pH fiber are tilted with respect to the fiber axis. This interpretation is supported by simulated fiber diffraction patterns calculated from models of the packing of tilted virions. The diffraction patterns from fibers of some mutants of fd, and from other wild-type strains of *Inovirus* (M13, IKe, If1), do not show layer-line fanning. We propose that the tilting of crystallites that gives rise to layer-line fanning in fd fibers is due both to a specific pattern of charge on the surface of the fd virion at higher pH and to the presence of a specific inter-subunit hydrogen bond. Apparently these features of the fd virion structure require a strict 2-fold screw axis along the virion axis that affects the packing between neighboring virions, resulting in the formation of a tilted smectic liquid crystal phase.

1. Introduction

Inovirus (filamentous bacteriophage) is a well-characterized biological semiflexible (wormlike) polyelectrolyte about 6 nm in diameter and 1000 nm long. The virion comprises a coat of several thousand identical protein subunits in a helical array surrounding a DNA core, with a few minor proteins capping the two ends of the virion. *Inovirus* has been extensively studied by techniques of molecular biology, and many different strains and mutants have been isolated, making the system a unique model for studies of macromolecular interactions and liquid-crystalline behavior. For instance, it is possible by simple biological manipulations to prepare sets of monodisperse virions with different surface charge densities or with different lengths (from about 20 to 2000 nm) but the same surface charge density.

In concentrated solutions the virions form birefringent liquid-crystal domains or crystallites. The crystallites can be aligned parallel to one another by mechanical means such as fiber-drawing and/or by magnetic or electric fields. In the best-aligned fibers, the disorientation half-width is less than 1°. This property has enabled detailed X-ray fiber diffraction studies that have led to precise molecular models for the virion.[1−3] The protein subunits in the virion are slightly curved α-helices. Each subunit has about 50 amino acid residues and has a mass of about 5000 amu (the details vary from one strain to another). The subunits are about 1 nm wide by 7 nm long, arranged in an overlapping interdigitated array, with their long axes at a small angle to the virion axis (Figure 1).

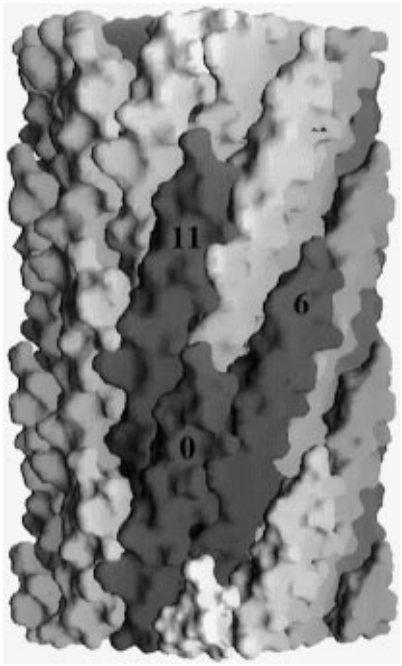

Figure 1. Model of the fd virion. The molecular surface[39] of the virion is displayed using the program GRASP.[40] Three neighboring subunits are shown in darker gray. These subunits are indexed[2] as 0 (center), 6 (right), and 11 (left). The diameter of the virion is about 6 nm. A slab about 10 nm long is shown, cut from the full 880 nm length of the virion in the diad symmetry, model 1IFJ. The virion axis is vertical, with the N terminus of each subunit toward the top. The C-terminal region of each subunit is hidden by overlapping neighbors.

* Author to whom correspondence should be addressed.
[†] Cavendish Laboratory, University of Cambridge.
[‡] Cambridge Centre for Molecular Recognition, University of Cambridge.
[§] CLRC Daresbury Laboratory.
[⊗] Abstract published in *Advance ACS Abstracts,* September 15, 1996.

S0024-9297(96)00561-X CCC: $12.00

Two symmetry classes have been identified on the basis of X-ray fiber diffraction patterns of various strains of *Inovirus*. Class II, typified by strain Pf1, is a simple helix in which successive protein subunits are related by a translation parallel to the helix axis of 2.9 Å and a rotation around the axis of 66.67°. For class I, typified by the Ff group (strains fd, f1, M13), five subunits are related by a 5-fold rotation axis around the helix axis, and such pentamers are successively related by a translation parallel to the helix axis of about 16 Å and a rotation around the axis of about 182.7° (for the "canonical" class I symmetry) or precisely 180.0° (for the "diad" class I symmetry). The canonical symmetry is so named because several unrelated strains show this symmetry, so it appears to be a general property of class I virions. Despite the differences between the class I and class II symmetries, the shape and local packing of the subunits are surprisingly similar for the two classes. There are acidic amino acid residues on the outer surface of the virion; basic residues lining the inner surface of the protein shell, where they neutralize the negative charge on the DNA core; and apolar residues buried in the interior of the protein shell, which are involved in interactions between subunits. The isoelectric point (p*I*) of the fd virion occurs at about pH 4 (refs 4 and 5).

In fibers with less than about 75% water content by volume, the virions pack in a hexagonal or pseudohexagonal lattice. These fibers give sharp crystalline reflections on the equator that may extend as far as 8 Å resolution for the drier fibers (about 15−20% water content). These equatorial crystalline reflections define a hexagonal net with a single virion passing through it parallel to the fiber axis. Less well-defined crystalline reflections on off-equatorial layer lines are also observed for some diffraction patterns. In most cases the off-equatorial reflections can be indexed on a real-space unit cell with 3 times the area of the unit cell defined by the equatorial reflections. This indicates that three virions pass through the "true unit cell", and that they have different relative translations along and/or rotations around the virion axis.[6,7]

Crystalline reflections on fiber diffraction patterns of the fd strain of *Inovirus* at higher pH (above p*I*) cannot however be indexed using this simple lattice,[7] and it has even been proposed that the crystalline reflections are not crystalline reflections at all, but instead are maxima in the continuous transform of large helical aggregates.[8] Here we show that the crystalline reflections on the equator can still be indexed on a hexagonal lattice, but the layer lines show "fanning".[9] That is, each apparent layer line actually consists of many layer lines lying at a small angle to one another. This happens because the layer lines from each crystallite in the fiber lie at slightly different angles to the meridian, which is a result of the crystallites being tilted with respect to the fiber axis.

Here we use our molecular model of the virion to analyze diffraction patterns with fanning, and we consider how small changes in the surface properties of the virion may generate changes in the packing of virions and thereby cause fanning.

2. Experimental Section

2.1. Materials. Virions were grown and purified using standard methods, including purification by 5% polyethylene glycol precipitation, sedimentation, and CsCl density-gradient centrifugation.[10] The homogeneity of virion solutions was confirmed by electrospray mass spectrometry after alkaline denaturation. Virion concentration was determined using an extinction coefficient of 3.84 mg^{-1} mL cm^{-1} at 269 nm for wild-type fd and 3.59 mg^{-1} mL cm^{-1} for mutants with one or two fewer tyrosines per subunit than wild-type fd.

Solutions of purified virions (7−10 mg/mL) from CsCl gradients were extensively dialyzed against 0.5 M NaCl and finally against 10 mM Tris-HCl, pH 8.0, containing 1 mM NaEDTA (TE buffer). Concentrated solutions were prepared by differential centrifugation at 15 °C: large aggregates were removed (20 min at 38000*g*), the virions were sedimented completely (4 h at 150000*g*) and then resuspended at about 75 mg/mL in TE buffer. Solutions with added 0.02% sodium azide could be stored at 4°C for up to several months before preparation of fibers. To prepare lower pH fibers, virion solutions were dialyzed against glycyl glycine buffer at pH 3.0 at very low virion concentration to minimize aggregation as the solution passed through the p*I* and then reconcentrated.

Fiber preparation and X-ray diffraction techniques were essentially as described for the Pf1 strain.[11] A drop of virion solution (30 mg/mL) in TE buffer was suspended across a 2.2 mm gap between the tips of two aligned siliconized wax-sealed glass capillaries (Durrum Microcaps, 0.8 mm diameter). Fibers were formed during drying for 30 h at 92% relative humidity (rh) in the sample chamber of a 9 T superconducting magnet with a room temperature bore. Fibers were stored at 75% rh. Gel samples[12] were produced by rehydrating fibers in 0.5 mm diameter quartz capillaries. Excess water causes the fiber to swell to the full diameter of the capillary in 10−20 min.

2.2. X-ray Diffraction. X-ray diffraction patterns were obtained on beamline 7.2 at the Synchrotron Radiation Source, Daresbury Laboratory, using a wavelength of $\lambda = 1.488$ Å. The specimen-to-detector distance (ca. 15 cm) was determined accurately by dusting silicon powder onto the fiber and measuring the ring at 3.136 Å. A flat plate fiber camera was used with a helium path and 0.2 mm collimator. The water content of the fiber was controlled by adjusting the relative humidity of the helium surrounding the fiber. Fiber patterns were collected either using a film pack, which was digitized with a Scandig3 microdensitometer on a 50 μm raster (0−2 optical density range); or on a 180 mm diameter MAR Research phosphor image plate. Diffraction data were measured and mapped from detector space to reciprocal space essentially as described for Pf1 *Inovirus*[11,13] using the CCP13 software suite (available on the world wide web at http://ncdfs1.dl.ac.uk/CCP13/).[14]

3. Theory

3.1. Calculated X-ray Diffraction Patterns. The Fourier-Bessel transform in a vacuum of a helix is[15,16,17]

$$G(R,\Psi,Z) = \sum_n \sum_j f_j(D) J_n(2\pi R r_j) \exp 2\pi i(Z z_j - n\phi_j) \exp 2\pi i n(\Psi + {}^1/_4) \quad (1)$$

where (r_j, ϕ_j, z_j) are the cylindrical polar coordinates of the jth atom in the asymmetric unit of the helix, (R, Ψ, Z) are the cylindrical polar coordinates of a point in reciprocal space (dimensions of ϕ_j and Ψ are fractions of a turn), and $f_j(D)$ is the atomic scattering factor of the jth atom at reciprocal spacing

$$D = (R^2 + Z^2)^{1/2} = 2 \sin \theta/\lambda \quad (2)$$

where 2θ is the diffraction angle and J_n is the Bessel function of order n. The reciprocal space coordinate Z is constrained by the helix selection rule

$$Z = l/c = n/P + m/p \quad (3)$$

where m is an integer, P is the pitch of the helix, and p is the unit rise between subunits in the helix. It is convenient in some cases to define a rational approximation using the smallest integers u and t such that $p/P = t/u$ within experimental error. Then there are integral numbers u units and t turns in the helix

repeat $c = up = tP$, diffracted intensity is limited to layer lines with $l = Zc$, and the selection rule becomes $l = tn + um$. For a nonintegral helix, the formal value of c may be very large (for instance for the canonical class I symmetry[2] $c = 1040$ Å), so we use conventions introduced in ref 18. A nonintegral layer-line index "l" $= ZP$ is defined by the helix pitch, P. For qualitative discussions, we refer to sets of overlapping layer lines with similar "l" values by zeroth layer line, first layer line, second layer line, etc. If there is an N-fold rotation axis along the helix axis, then n must be an integral multiple of N.

There will be no interference between low-order Bessel function terms if each Bessel function order n is assigned to a different layer line l by eq 3. This is the case for the canonical class I symmetry, but it will also be true for any symmetry that differs from perfect diad class I symmetry, however slightly. In this case, the molecular transform $G(R,\Psi,Z)$ (eq 1) on any layer line $l = Zc$ and at any reciprocal space radius R will have the same amplitude for all Ψ around the layer plane. On the other hand, if two or more Bessel function terms interfere on the same layer line, the molecular transform will vary around the reciprocal space layer plane at constant R as a function of the azimuthal angle Ψ. The amplitudes of crystalline reflections depend on the underlying molecular transform of the virion, so one can visualize the crystalline reflections as sampling the varying molecular transform at the crystal lattice points. If there is no specific packing between virions, they will diffract as individuals. Then the molecular transform will be cylindrically averaged around Ψ, and the variation with Ψ will not be experimentally detectable.

To compare simulated diffraction from *Inovirus* with observed data, the calculated molecular transform of the helical protein shell must be extended to include the contribution of the DNA. The DNA does not have the same helix symmetry as the protein shell and comprises only about 10% by weight of the virion, so we include only a J_0 contribution on the equator, corresponding to a cylindrically symmetrical DNA distribution in the virion core. We also take into account the presence of solvent surrounding the virion, since the changes that we wish to analyze occur at relatively low resolution, where diffraction due to solvent has a significant influence. From the transform of the virion with respect to a vacuum we subtract the transform of the molecular volume of the virion filled with a uniform density of 0.334 e/Å^3, the electron density of water, to give the transform of the virion relative to water.[2,13]

To calculate simulated diffraction patterns we calculate the molecular transform (with DNA and solvent correction) of a molecular model from eq 1. For the canonical symmetry we use protein data bank[19] entry 1IFI and for the diad symmetry, entry 1IFJ. The local structure of the subunit is similar for the two models, but the subunit shape and orientation is affected by the interlocking of neighboring subunits.[2] Both models are based on a pentamer of protein subunits related by a 5-fold rotation axis along the z axis (the virion axis). For the diad symmetry there are precisely two pentamers per turn of a helix with $c = 32.2$ Å. By eq 3, layer lines of even order ($l = 0, 2, ...$) only have values of $G(R,\Psi,Z)$ for which $n = 0, \pm10, \pm20 ...$, and odd layer lines ($l = 1, 3, ...$) only have values of $G(R,\Psi,Z)$ for which $n = \pm5, \pm15, ...$ For the canonical symmetry the layer lines are "split" slightly from their positions on the diad diffraction pattern (except $n = 0$ on $l = 0$, which is unchanged).[2] For instance, on $l = 1$ for the diad symmetry, $G(R,\Psi,Z)$ contributes for both $n = +5$ and $n = -5$ with $R < 0.15$ Å^{-1}, and interference between these terms is expected. For the canonical symmetry, the layer line carrying the $n = 5$ term is moved to "l" $= 1.06$, and the layer line carrying the $n = -5$ term is moved to "l" $= 0.91$, so interference between these two terms cannot occur.

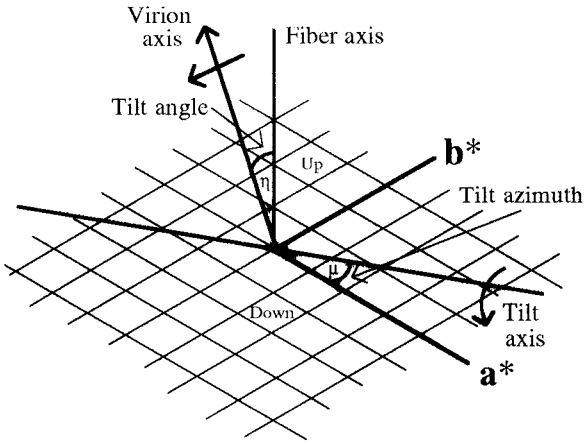

Figure 2. Displacement of reciprocal lattice points in a fiber diffraction pattern by tilting. A plane reciprocal lattice defined by vectors **a*** and **b*** is tilted so the virion axis makes an axial tilt angle η with the fiber axis. The orientation of the tilt axis in the **a*****b*** plane is defined by the azimuthal tilt angle μ measured from the **a*** vector. The azimuthal tilt axis remains in the **a*****b*** plane. The virion axis remains perpendicular to the azimuthal tilt axis and to the **a*****b*** plane. Our sign convention for the angles η and μ is such that in the diagram the sign of the tilt angle η is positive, while that of the azimuthal angle μ is negative. Reflections on one side of the tilt axis are displaced above the layer line position of an untilted fiber pattern; reflections on the other side are below this position. Reflections farther from the axis are displaced more than those nearer the axis. Only the $l = 0$ layer plane is shown, for clarity; analogous effects occur for higher layer planes (after ref 25).

If the helices pack in a crystalline unit cell, the structure factor at crystal lattice point hkl is[15]

$$F(hkl) = \sum_h G(R,\Psi,Z) \exp 2\pi i(hx_h + ky_h + lz_h - n\phi_h) \quad (4)$$

where (x_h, y_h, z_h) are the fractional coordinates of the hth helix in the unit cell, and ϕ_h is the relative rotation of the hth helix around its own axis in fractions of a turn. The lateral positions of the virions (x_h, y_h) can be determined from the equatorial reflections. The rotations ϕ_h and axial translations z_h can only be determined if n and l are not equal to 0. For the diad symmetry, multiple Bessel functions contribute to $l = 1$. This makes it difficult to determine the relative ϕ_h, z_h of the virions directly, but one can calculate the structure factors $F(hkl)$ for trial packing arrangements to search for a packing that explains the observed distribution of crystalline reflections.

A conventional fiber pattern is analogous to a single crystal rotation pattern. Since the crystallites are randomly oriented around the direction of the long axis of the molecule, which by convention is taken as the **c** real lattice vector, all crystalline reflections hk on a layer plane with the same reciprocal space radius R are superimposed on the fiber pattern. But if the crystallites are tilted with respect to the fiber axis, the **c** axis of the unit cell is not parallel to the fiber axis, so the **a*****b*** plane of the reciprocal lattice is not perpendicular to the meridian on the fiber pattern (Figure 2). Such a fiber pattern is analogous to a mis-set single crystal

rotation pattern,[20] and individual reflections that would be superimposed on a normal fiber pattern may be resolved. The mis-setting of the crystallites is defined by the axial tilt angle η and the azimuthal tilt angle μ, as shown in Figure 2. In discussing these fiber patterns, we use the terms "equator" and "meridian" to refer to the directions on the diffraction pattern that are perpendicular and parallel, respectively, to the fiber axis direction, but note that for fiber patterns of tilted crystallites, some reflections that index on $l = 0$ are not on the equator by this definition. The CCP13 program LSQINT[14] can calculate simulated diffraction patterns for crystallites that are tilted as shown in Figure 2.

To generate simulated crystalline fiber patterns, we need to take into account several effects, caused by the finite size of the crystallites, that modify the ideal shape of the crystalline reflections. These include disorientation (which spreads diffracted intensity along an arc of constant D), finite particle coherence length (which broadens layer lines in Z), finite particle coherence width (which broadens all reflections equally in R), and variation in the lateral unit cell dimensions from one crystallite to another (which broadens reflections in proportion to the reciprocal space radius R). These modifications to the shape of the crystalline reflections and the correction for the Lorentz effect are made using LSQINT. We determine the values of these parameters from observed fanned diffraction patterns by measuring the observed layer line breadth near the meridian, where disorientation has little effect, and by measuring the observed breadth of equatorial reflections for low and high resolution and making a linear interpolation. After making these modifications to the simulated pattern, we add the appropriate disorientation correction by inspection. Even for simulated patterns it can be difficult to identify and index particular nonequatorial hkl reflections after these modifications have been applied, so for tilted crystallites we refer not to "crystalline reflections" but instead to "spots" of intensity, which may comprise several crystalline reflections.

Disorder in the packing of the virions in a fiber can result in a diffraction pattern with a mixture of crystalline reflections and continuous transform.[21,22] "Lattice disorder" may involve small random lateral translations and/or small axial translations of the virions from the average lattice positions. "Substitution disorder" may involve axial translations and/or rotations of the virions, or inversion in the direction of the virions ("up/down" disorder) within an unchanged unit cell. The effect of lateral, axial, and rotational disorder is to increase the intensity of the continuous transform at the expense of that of the crystalline reflections with increasing R, Z, and n, respectively. Both lattice and substitution disorder will change the extent and intensities of crystalline reflections, but not their positions in reciprocal space. In our simulated crystalline fiber diffraction patterns we have not attempted to include the effects of this disorder on the calculated $F(hkl)$. We model the disorder separately, using the methods developed by Stroud and Millane.[21] These methods involve an extension of the classical model of disorder of the first kind.[23] In this model the random displacements of the virions from average lattice positions are independent and therefore are uncorrelated.

4. Results

4.1. Crystallographic Evidence for a Tilted Lattice. Crystalline reflections from diffraction patterns of *Inovirus* can be indexed on a hexagonal lattice.[6,7] The

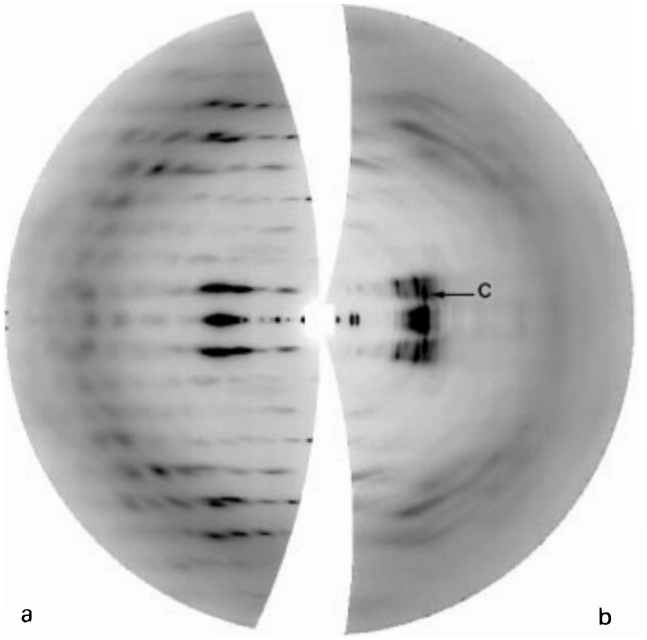

Figure 3. X-ray fiber diffraction patterns of *Inovirus*. The fiber axis is vertical. The diffraction patterns were mapped from detector to reciprocal space and quadrant averaged. The diffraction patterns shown consist of the averaged quadrant mirrored across the equator. The outermost edge of the patterns has a spacing of 0.32 Å^{-1}. The central blind area differs on the two patterns because the fiber tilt was different. (a) Diffraction pattern of a fiber of a Y21M mutant, which is equivalent to the lower pH fiber of wild-type fd; image number, py21mgel001; fiber number, PY28. (b) Diffraction pattern of a higher pH fiber of wild type fd: film number, 343b; fiber number, F3TA26.

crystalline reflections on $l = 0$ define a hexagonal layer plane with one virion at each lattice point. For the class I strains If1 and IKe, the higher layer lines can only be indexed on a unit cell with three molecules passing through it and with the first layer line split according to the canonical helix symmetry. For this larger unit cell, there are systematic absences on $l = 0$ for $n = 0$, and three virions passing through the unit cell having the following fractional (x, y, z, ϕ) coordinates: ($^1/_3$, $^1/_3$, z_1, ϕ_1), ($^2/_3$, 0, z_2, ϕ_2), and (0, $^2/_3$, z_3, ϕ_3).

All of the observed equatorial reflections on the higher pH fd patterns can also be indexed on this lattice.[7] This indexing is not consistent with the helical aggregate model[8] because the positions of these peaks of intensity do not correspond with maxima in the continuous transform of helical aggregates. Attempts to index the nonequatorial reflections using the hexagonal lattice symmetry derived from the equatorial reflections were unsuccessful.[7] The higher pH (pH > pI) and lower pH (pH < pI) fd fiber patterns (Figure 3) both show the characteristic strong intensity at 10 Å in the equatorial direction and at 5 Å in the meridional direction, indicating that the α-helix structure of the virion does not change with pH. The $^1/_{32}$ Å^{-1} periodicity of the layer lines is also very nearly the same, indicating that the helix symmetry is not significantly changed. But there is a clear splitting of the layer lines in the lower pH pattern, particularly visible on the first (Figures 3a and 4a) and the fifth and sixth layer lines (Figure 3a). There are also crystalline reflections on the first layer line of the lower pH fd pattern, and these crystalline reflections can be indexed on a hexagonal lattice, as for If1 and IKe.

The higher pH fd patterns do not show clear layer-line splitting, and the layer lines are generally less well

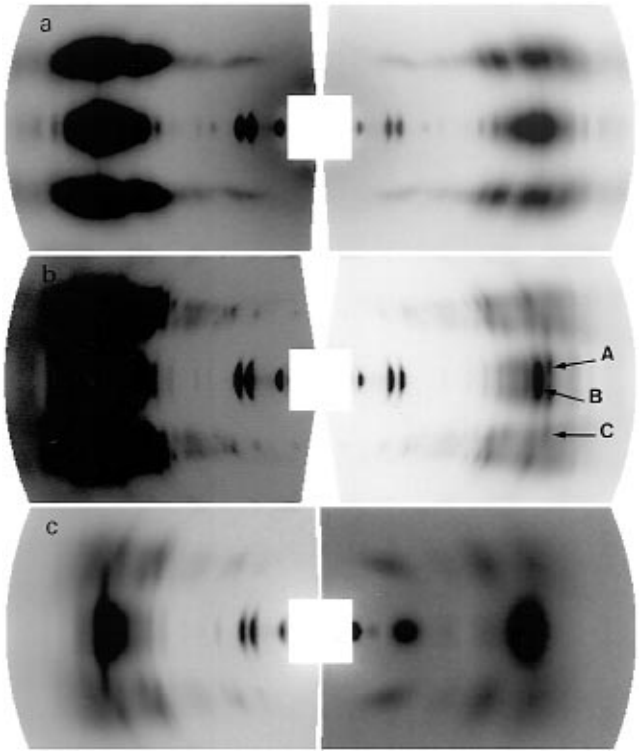

Figure 4. X-ray fiber diffraction patterns of *Inovirus*, as in Figure 3 but showing only the central region, (the zeroth and first layer lines), on an expanded scale. For parts a and b, the right side is the same pattern as the left side, but less heavily exposed to show detail in the more intense regions. (a) Diffraction pattern of a fiber of a Y21M mutant as in Figure 3a: film number, 335b; fiber number, G3YT14. (b) Diffraction pattern of a higher pH wild-type fd fiber as in Figure 3b: particular diffraction spots are marked A, B, and C; film number, 280b; fiber number, F3TA54. (c) Diffraction pattern of a higher pH wild-type fd fiber: (left) dry fiber, similar to Figure 3b; film number, 325b; (right) same fiber after hydrating to form a gel; film number, 327b; fiber number, F3TA48.

defined than for the lower pH patterns. Where there are crystalline reflections, they are generally superimposed on a background of continuous molecular transform. Some $l = 0$ spots have weaker intensity on the equator than on either side of the equator, and the intensity of spots on $l = 1$ is not symmetric about the mean layer line position (Figures 3b and 4b). Such effects are known for fibers in which crystallites are tilted slightly with respect to the fiber axis, causing the layer lines to fan into wedge shapes.[23−25] For fibers of the synthetic polymer poly(ethylene−terephthalate),[25] the lattice is triclinic, so there would be no superposition of reflections even in a normal fiber pattern. The tilt simply causes the reflections to move to new positions on the fiber pattern. Fiber patterns of collagen also show layer-line fanning.[9,26,27] The equatorial spots on the higher pH fd pattern resemble those of collagen fibers, in that some spots show a break in the center of an otherwise continuous arc. This is a result of the collagen molecules lying at an angle to the fiber axis.[27]

We consider three possible types of tilting to explain the diffraction patterns of fd at higher pH.

(I) The lattice is hexagonal but the **c** vector of the real lattice lies at a small angle to the fiber axis. In this case the **c*** vector of the reciprocal lattice is not parallel to the meridional direction. The **a***-**b*** planes (the layer planes) are perpendicular to the **c*** direction and are not parallel to the equatorial direction on the fiber pattern (Figure 5a). A normal fiber pattern (Figure 3a) can be thought of as a special case of type I tilting where the angle between the fiber axis and the **c** axis is equal to zero.

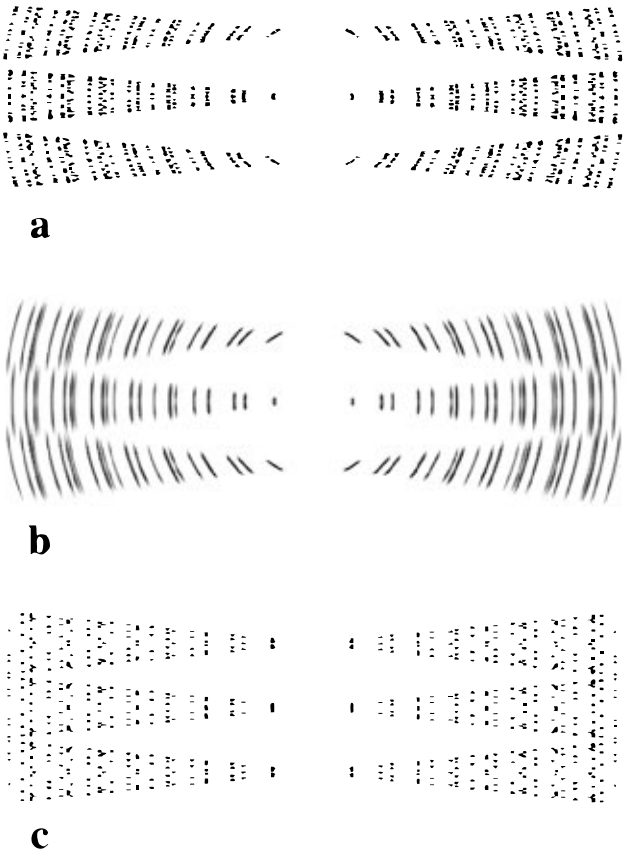

Figure 5. Calculated positions of crystalline reflections on fiber patterns for different unit cell tilt types. Central region, as in Figure 4. The simulated diffraction patterns were generated using the computer program LSQINT, with all *F(hkl)* set to the same constant value. In all cases the space group is *P*1. (a) Tilt type I with negligible disorientation; hexagonal unit cell, with $a = b = 60.0$ Å and $c = 32.3$ Å, with disorientation of 0.002°, particle coherence length of 0.0005 Å^{-1}, and particle coherence width of 0.001 Å^{-1}. The unit cell tilt axis parameters are $\mu = -49°$ and $\eta = -5°$. (b) Tilt type I, with appreciable disorientation. Parameters as in part a, except that the disorientation is 1.0°. (c) Tilt type II, with disorientation and particle coherence length parameters as in part a; triclinic unit cell, with $a = b = 60.0$ Å, $c = 32.3$ Å, $\alpha = 85.0°$, $\beta = 90.0°$, and $\gamma = 120.0°$. The unit cell **c*** axis is parallel to the fiber axis.

(II) The **ab** plane of the real lattice is perpendicular to the fiber axis, but the lattice is not perfectly hexagonal, so the virion axis (defined as the direction parallel to the **c** vector of the unit cell) is not parallel to the fiber axis. That is, at least one of the α, β angles of the pseudohexagonal unit cell is not equal to 90°. The **a***-**b*** planes are not parallel to the equatorial direction on the fiber pattern, but the **c*** axis is parallel to the meridional direction. The crystallite tilt angles η and μ are functions of the unit cell parameters and are not independent variables as they are for tilt types I and III (Figure 5c).

(III). The lattice is tilted as in type I, so the **c** vector makes a small angle with respect to the fiber axis, but the lattice is not perfectly hexagonal (i.e. the unit cell parameters are slightly different from those that define a hexagonal unit cell). In this case, the **a***-**b*** planes are not perpendicular to the **c*** direction. The layer planes are not parallel to the equatorial direction on the fiber pattern, and the *hk* reflections that lie on arcs of constant *D* for tilt type I do not do so for tilt type III.

Tilt type III is the general case, type II is a special case of type III with the **c*** axis parallel with the meridian, and type I is a special case of type III with a hexagonal lattice. All three types of tilting spread crystalline reflections that would otherwise be superimposed on an untilted fiber pattern, but the detailed nature of this spreading is different for the different types. Disorientation of the crystallites causes adjacent fanned crystalline reflections to merge, so individual reflections are not resolved, as shown for the case of type I tilting in Figure 5b.

Even when the individual crystalline reflections are not resolved, we may still be able to distinguish between the three types of possible crystallite tilt. The fanned layer lines from tilt type II are symmetrical about the mean layer-line position (i.e. the layer-line position if there were no lattice tilt) (Figure 5c). However, the layer-line fanning from tilt type I results in a pattern of nonequatorial layer lines that are not symmetrical about the mean layer-line position (Figures 5a,b). This is also the case for fanning from tilt type III. The observed nonequatorial layer lines of the higher pH fd diffraction pattern are not symmetrical about their mean positions (Figure 4b), so tilt type II is ruled out. This is independent of any disorientation and results from the **c*** direction being at an angle to the fiber axis.

The disorientation in the fiber precludes the resolution of the individual crystalline reflections, so the azimuthal tilt angle μ cannot be determined precisely.[24] However, the axial tilt angle η can be estimated from the fiber pattern by fitting a straight line to the top and bottom edges of a fanned layer line in reciprocal space. This procedure gave an axial tilt angle of $\eta = 6.5 \pm 0.4°$, which is a slight overestimate because of disorientation (Figure 4b). We have found no significant change in the axial tilt angle with relative humidity.

4.2. Diad Symmetry of the Virion. For the perfect diad symmetry, there is interference between different Bessel function terms for a given l, and the molecular transform of the virion varies with Ψ around the layer plane, as illustrated in Figure 6. In the region of strong intensity at $R \cong 0.1$ Å^{-1} on $l = 0$, the transform has 10-fold periodicity in Ψ, but the layer plane of a hexagonal reciprocal lattice has 6-fold rotational symmetry. Thus at any radius, R, some of the reciprocal lattice points will sample strong regions of the molecular transform, and others will sample weaker regions. For a normal fiber pattern, reflections with the same reciprocal space radius R are superimposed. Tilting the crystallites can separate reflections that are at the same radius but have different hk, as illustrated in Figure 2. Lattice points that index on $l = 0$ and also lie on the azimuthal tilt axis of Figure 2 will lie on the equator of the diffraction pattern. Lattice points off the azimuthal tilt axis will be off the equator, even if they index on $l = 0$. If the azimuthal tilt axis passes through one of the maxima at $R \cong 0.1$ Å^{-1} on Figure 6, then a lattice point on or near the tilt axis will have high intensity on the equator of the diffraction pattern, for instance spot B on Figure 4b. Neighboring regions, where the lattice points nearest the tilt axis lie on minima, may have weak intensity on the equator, for instance, spot A on Figure 4b. We use these considerations to estimate that the azimuthal angle is about $\mu = -49°$.

On $l = 1$ the crystalline reflections that are observed will depend on the fractional z translations and ϕ rotations of the three virions in the unit cell. For some fibers of strain If1 in the canonical symmetry, there are systematic absences on the first layer line for $h - k = 3q$, with q any integer. That is, those reflections that

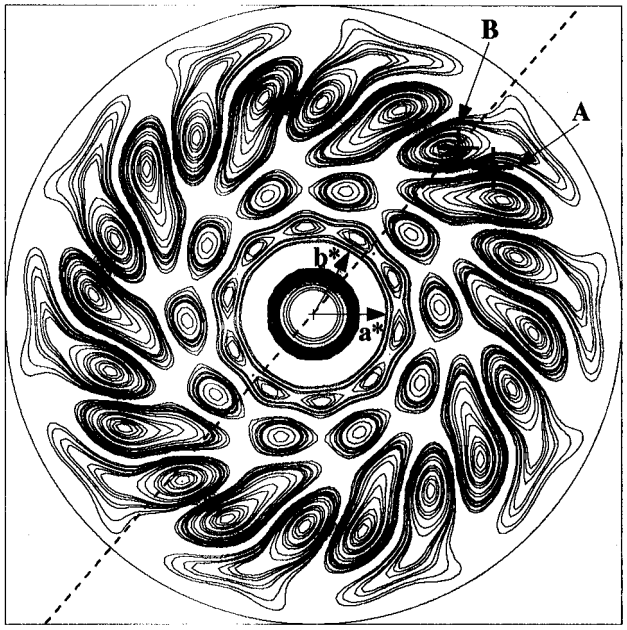

Figure 6. Distribution of the calculated molecular transform on the $l = 0$ layer plane for a single fd virion with interference between Bessel function terms. The molecular transform $|G(R,\Psi,Z)|^2$ of the diad model 1IFJ was calculated from eq 1, including DNA and solvent correction, using Bessel function orders to $n = \pm 20$. $R = 0.0$ Å^{-1} is at the center of the box, with Ψ measured counterclockwise from the **a*** axis. The half-width of the box is 0.15 Å^{-1}. The azimuthal tilt axis for $\mu = -49°$ is shown as a dashed line. The reciprocal lattice points $hkl = 470$ and $hkl = 280$, corresponding to diffraction spots A and B, respectively, that lie closest to the azimuthal tilt axis are shown.

are present on the equator are systematically absent on the first layer line, and *vice versa*.[7] These systematic absences can be explained by certain combinations of the relative translations Δz and relative rotations, $\Delta\phi$, of the virions in the unit cell, given by[6]

$$l\Delta z - n\Delta\phi = q'/3 \qquad (5)$$

where q' is an integer not equal to $3q$. As mentioned in the previous section, the nonequatorial reflections in the higher pH fd patterns cannot be indexed on this lattice, but as a first approximation for $l = 1$ with fd in the diad symmetry, we use a simple relation derived from the If1 case, $\Delta z = {}^1/_3$, $\Delta\phi = 0$ (Figure 7a).

As well as $\Delta z = +{}^1/_3$, we have tried other options with $\Delta\phi = 0$: $\Delta z = -{}^1/_3$, $\Delta z = \pm{}^1/_2$, and $\Delta z = 0$ (i.e. one virion per unit cell). The $\Delta z = \pm{}^1/_3$ and $\Delta z = 0$ options give strict systematic absences on $l = 1$, whereas other options permit additional reflections. It is likely that there will be virions pointing in both directions ("up" and "down" with respect to the fiber axis) in the crystallites, and if there are specific spatial relationships between "up" and "down" virions, there will be intensity changes on nonequatorial layer lines of the diffraction pattern. It is difficult to decide between these alternatives for fd from our diffraction patterns, so we use $\Delta z = {}^1/_3$, $\Delta\phi = 0$ with no "up/down" disorder for our simulations.

All these simulated patterns based on a strictly hexagonal tilted unit cell (tilt type I) fail to reproduce one striking feature of the observed diffraction pattern, a spot that extends downward from $l = 1$ toward the equator (spot C on Figure 3b; Figure 4, part b; and Figure 4, part c, left). Slight distortion of the hexagonal unit cell (tilt type III) reproduces this feature. A simulated diffraction pattern of the virion with diad

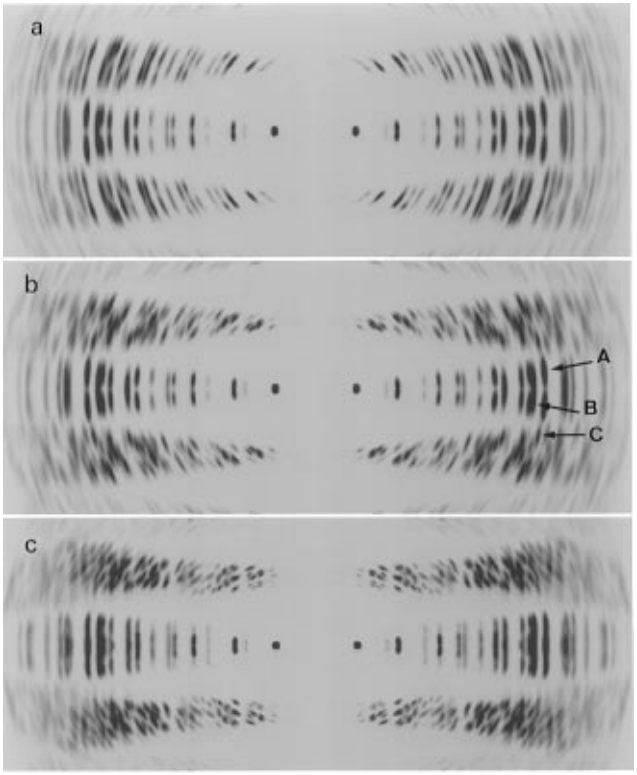

Figure 7. Simulated X-ray fiber patterns of fd. The central region as for the observed patterns of Figure 4. The transform of a model was calculated, including the DNA contribution and the solvent correction. Three virions pass through the unit cell, with fractional coordinates as given in section 4.2, in space group *P*1. In all cases a particle coherence length of 0.0007 $Å^{-1}$ was used, and the width (RWIDTH) of the crystalline reflections is given by RWIDTH = R0WI + R1WI × *R* (ref 14), where R0WI = 0.00128 $Å^{-1}$ and R1WI = 0.00438 $Å^{-1}$. (a) Diad symmetry, model 1IFJ; hexagonal unit cell with parameters $a = b = 102.0$ Å and $c = 32.3$ Å. The unit cell tilt axis parameters are $\mu = -49°$ and $\eta = -5°$, the disorientation is 1.6°. (b) Diad symmetry, model 1IFJ; skew hexagonal unit cell with $a = 102.6$ Å, $b = 103.1$ Å, $c = 32.9$ Å, $\alpha = 82.1°$, $\beta = 94.9°$, and $\gamma = 120.5°$. The unit cell tilt axis and disorientation parameters are the same as for part a. Spots corresponding to A, B, and C of Figure 4b are indicated. (c) Canonical symmetry, model 1IFI; skew hexagonal unit cell with $a = 102.6$ Å, $b = 103.1$ Å, $c = 208.0$ Å, $\alpha = 82.1°$, $\beta = 94.9°$, and $\gamma = 120.5°$. The unit cell tilt axis parameters are $\mu = -49°$ and $\eta = -4°$, and the disorientation is 1.0°.

symmetry in the slightly distorted hexagonal unit cell (tilt type III) is shown in Figure 7b. Spots A−C on the observed diffraction pattern are reproduced on this simulated pattern. As mentioned above, the crystalline reflections for tilt type III do not lie on arcs of constant *D*. The resulting diffraction pattern is much more complicated than for tilt type I. This problem, combined with the presence of underlying continuous transform intensity, means that it is currently not feasible to index reliably the observed nonequatorial spots.

For the canonical symmetry, there is no interference between Bessel function terms, and the zeroth layer line is split into two adjacent layer planes. Some broad regions of the diffraction pattern have low intensity on the equator and higher intensity off the equator, and other regions have the reverse. But adjacent weak and strong equatorial spots on a skew tilted lattice, like spots A and B of Figure 4b, are not reproduced (Figure 7c). The overall intensity distribution is similar to the simulated patterns for the diad symmetry (Figure 7b), but the edges of the layer lines are less regular than in the observed diffraction patterns (Figure 4b) as a result of the layer line splitting. There is less variation in intensity along the first layer line arcs in the simulated canonical pattern (Figure 7c) than in the observed pattern (Figure 4b), although this varies slightly with the azimuthal tilt angle. We conclude that the observed fanned diffraction patterns are best explained by fd virions in the diad symmetry, arranged in crystallites having tilt type III.

4.3. Other Evidence for Tilted Crystallites. Further support for the tilted crystallite model comes from an experiment in which a higher pH fd fiber was placed in a thin-walled quartz capillary and X-ray diffraction patterns were recorded before and after distilled water was added to the fiber (Figure 4c). The usual fanned pattern is obtained from the dry fiber, but after the fiber has swollen to form an oriented gel, the apparent width of the layer lines decreases. Normally one expects increased layer-line width when forming a gel from a fiber, because of increased disorientation in the gel, and this is indeed observed for fibers of virions that do not show fanning.[12] The decrease in apparent layer-line width when forming a gel from a higher pH fd fiber presumably results from the relaxation of the tilted virions in the lattice to a looser arrangement, spaced further apart, allowing the long axes to lie more nearly parallel to the fiber axis, thus reducing or eliminating the fanning.

An X-ray diffraction pattern of a section of a magnetically aligned higher pH fiber with the fiber axis parallel to the X-ray beam shows rings of uniform intensity (data not shown) that correspond in *D* to the equatorial crystalline reflections observed on fiber patterns with the fiber axis perpendicular to the X-ray beam. The circular uniformity of the rings indicates that there is no preferred axis of alignment of the crystallites about the fiber axis. The higher pH fibers have true fiber type order, not double orientation.[23]

The poor orientation of nonmagnetically aligned higher pH fibers prevents a detailed analysis of their diffraction patterns from being carried out. However, as the nonequatorial reflections of these nonmagnetically aligned fibers could not be indexed on a simple hexagonal lattice,[7] this suggests that the tilting of the crystallites arises from the intrinsic physical properties of the fd virion and is not induced by the magnetic field.

4.4. How Mutations Affect Fanning. On each fd coat protein subunit, one basic and four acidic side chains are exposed at the surface of the virion,[2] giving the virion a net negative charge of −3 e/subunit at neutral pH (ref 5), corresponding to a linear charge density of about −1 e/Å. The M13 strain, which does not show fanning, has the same coat protein sequence as fd except for the acidic Asp residue at position 12, which is replaced by uncharged Asn, so M13 has a net negative charge of −2 e/subunit at neutral pH. This correlation between fanning and surface charge suggested the successful tactic of lowering the pH below p*I* to eliminate fanning.[28] Fanning is also eliminated by another charge-change mutation in fd, Asp4 to Gly (unpublished result). In contrast, a Lys48 to Ala mutation of fd does not eliminate fanning,[12] but this is not surprising since residue 48 is buried within the virion, where it interacts with the DNA, and should not affect the surface charge.

The fanning effect does not however depend solely on surface charge. A mutation that changes Tyr21 to Met, leaving the surface charge unchanged, also eliminates the fanning,[2] as does a double mutation, Tyr21 to Phe plus Tyr24 to Ser (unpublished result). In our model of the fd virion, Tyr21 on each subunit of index $k = 0$ makes a hydrogen bond to Trp26 on a neighboring

subunit with index $k = +5$ (see Figure 10a of ref 2). However Tyr24 to Phe (ref 8) or Tyr24 to Met (unpublished result) mutation does not eliminate fanning. Wild-type strains If1 and IKe, which do not show fanning, have both a surface charge of only −2 e/subunit and a replacement of the Tyr at position 21 (ref 2).

We propose that the combination of a surface charge of −3 e/subunit and the Tyr21 to Trp26 inter-subunit hydrogen-bond constrains the virion to a region of conformational space for which the minimum energy of crystallization requires tilted crystallites of virions in the diad symmetry. Relaxing either the charge or the hydrogen bond relaxes this constraint and allows non-tilted packing.

4.5. Disorder in the Crystallites. Fiber patterns of all strains of *Inovirus* show continuous intensity overlaid with crystalline reflections at small diffraction angles, but elsewhere on the pattern, there is only continuous intensity on the layer lines. For fd, the lack of crystalline reflections on layer lines beyond the second layer line and the limited lateral extent of the observed reflections suggest that there is both axial and lateral disorder in the packing of the virions. This disorder is independent of the tilted crystallite model presented above, but should be considered when attempting to simulate diffraction patterns. To estimate the extent of lateral, axial, and rotational disorder required to reproduce the observed limitations on crystalline reflections, we calculate layer-line amplitude profiles for fd diad virions in a hexagonal lattice and explore the effect of varying the standard deviations of disorder on the diffraction pattern. We find that quite small amounts of lattice disorder are sufficient to suppress the crystalline reflections on all layer lines other than the zeroth, first, and second layer lines and at resolutions greater than about 8 Å (Figure 8). We estimate that the standard deviation of lateral disorder is between 1 and 2 Å. Values outside this range yield simulated patterns that are either more or less crystalline than the observed patterns. The small value of this variable is consistent with the close packing of virions in dry fibers.[7] Similarly, the standard deviations of axial and rotational disorders cannot be much greater than 3.5 Å and 5°, respectively. We have also explored the effects of various kinds of substitution disorder, but we find that it is the lattice disorder that makes the most important contribution to the elimination of crystalline reflections at higher resolution. This is in agreement with similar calculations for DNA fibers performed by Stroud and Millane.[21]

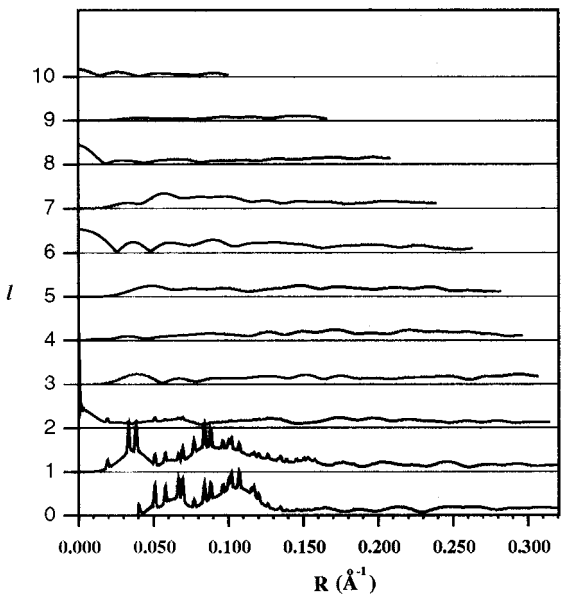

Figure 8. Amplitude distribution calculated for the semicrystalline lattice of fd, with disorder. The curves correspond to layer lines in one quadrant of the fiber pattern, with the meridian vertical and the equator horizontal. The layer line index l for $c = 32.2$ Å is shown to the left of each layer line. Amplitude $|G(R)| = I^{1/2}$, not intensity I, is plotted on each layer line to reduce the scale difference between strong and weak intensity. The transform of a single virion per hexagonal unit cell, with crystallite radius 390 Å, was calculated for model 1IFJ, using the computer program DISORDER.[21] DNA was not included in the calculation, and no correction was made for solvent. These features affect mainly $l = 0$ for $R < 0.04$ Å^{-1}, so this region is omitted from the figure. A temperature factor of B = 10.0 Å^2 was used for the calculation. The disorder was assumed to be normally distributed, with zero mean, and with standard deviations of 1.0 Å, 3.5 Å, and 5° for the lateral, axial, and rotational disorder, respectively.

5. Discussion

In the semicrystalline fibers formed by most strains of *Inovirus*, the virions lie parallel to the fiber axis in a hexagonal array. This characteristic has been observed for strains with a wide range of surface structure (that is, major coat protein amino acid sequence) and for a wide range of experimental conditions. In the few exceptions that we have discussed here, the virions pack in a regular array, but with their axes tilted slightly with respect to the fiber axis. The tilt is relaxed when the water content of the fiber is increased enough to relieve the virions from close contacts. Analysis of the crystalline reflections on the fd fiber patterns shows that the virions in the tilted crystallites have a precise screw diad along the virion axis.

Concentrated solutions of *Inovirus* form liquid crystals. Various types of liquid crystalline behavior have been reported for these solutions[29−32] resembling properties of other lyotropic cholesteric liquid crystals.[33−35] As the concentration of an isotropic solution is increased, the first kind of liquid crystal phase to be formed is the nematic phase, in which the virions are roughly parallel to one another, but there is no long-range order and the ends of the virions are not in register. As the concentration is increased further, a more ordered kind of liquid crystal phase may form, the smectic phase, in which not only are the virions parallel but their ends are in register, and the virions form layers roughly perpendicular to their long axes.

To understand the reason for the tilting of fd crystallites, it is helpful to imagine the microenvironment within a fiber of *Inovirus* as it dries and the concentration increases (Figure 9). The solution may first form the smectic C phase, in which the virions are tilted with respect to the layer but have no long-range order, and as the concentration increases, they form the smectic G phase, with the planes of the layers perpendicular to the fiber axis (Figure 9a). Alternatively, the virions might first form the smectic A phase, in which they are roughly perpendicular to the layers but have no long-range lateral order within the layer. Then, as the concentration increases, they form smectic B phase, with lateral order. The layers may subsequently tilt with respect to one another, forming the smectic G phase, and this would be the final state for most strains of *Inovirus*. Such behavior has been reported for other systems (see Figure 2.10 of ref 33). But if, for fd, the planes of the successive tilted layers then rotate with respect to one another, the virions in the crystallites would be tilted with respect to the fiber axis (Figure 9b).

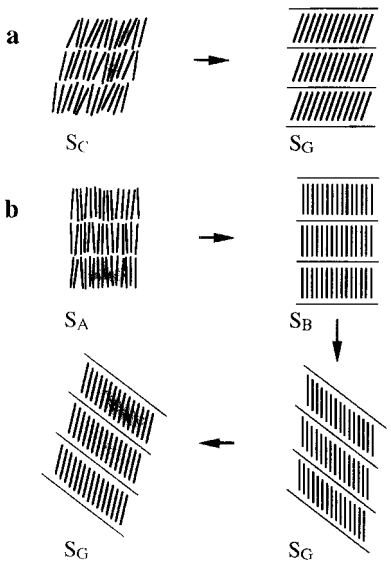

Figure 9. Models for possible liquid crystal behavior in fibers of fd. In all cases the fiber axis is vertical. The virions are represented by short lines; these form planar arrays as indicated by longer straight lines. (a) Transition from smectic C to smectic G and (b) transition from smectic A through smectic B to smectic G, followed by rotation of the smectic G planes around an axis normal to the planes. In this figure, to go from the third to the fourth section of part b, imagine the planes unchanged but the virions rotated by about 45° around an axis normal to the planes.

A smectic layer structure with a thickness of 0.83 to 0.86 μm was observed in cryoelectron micrographs of fd liquid crystals.[31] The length of the fd virion is 0.88 $\pm$ 0.03 μm (ref 36), and since there must be some space between the virions in adjacent layers, it is unlikely that the virion axis is exactly perpendicular to the smectic layers. The tilt angle that we derive from the X-ray patterns is consistent with this argument.

These considerations do not explain why wild-type fd virions should form tilted smectic liquid crystals whereas other strains of *Inovirus* do not. One possible explanation is that the unique combination of surface charge and internal hydrogen bonds causes the fd virion to lock into the perfect diad symmetry; as the concentration increases, this symmetry can only be accommodated in a pseudohexagonal unit cell that is tilted with respect to the smectic layers. Further studies on the electrical[37,38] and structural properties of fd as a function of ionic strength and virion concentration and further modeling of the packing of virions in the unit cell should help to resolve these questions.

Acknowledgment. We are indebted to Professor G. Cesareni for supplying some of the mutant *Inovirus* strains. We thank Dr. R. C. Denny for help with the CCP13 suite of computer programs, Professor R. P. Millane and Dr. W. J. Stroud for providing us with their computer software, Dr. W. Bras for help with magnetic alignment, Dr. J. Rodenburg for generous access to computer facilities, T. Terry for performing the mass spectrometry measurements, and G. E. Welsh for helpful discussions. This work grew out of the M. Phil. thesis of C. Dohle at the Cavendish Laboratory (1992). We are grateful to The Leverhulme Trust, The Wellcome Trust, and the Engineering and Physical Science Research Council for financial support. L. C. W. was supported by an EPSRC research studentship.

References and Notes

(1) Marvin, D. A. *Int. J. Biol. Macromol.* **1990**, *12*, 125.
(2) Marvin, D. A.; Hale, R. D.; Nave, C.; Helmer Citterich, M. *J. Mol. Biol.* **1994**, *235*, 260.
(3) Gonzalez, A.; Nave, C.; Marvin, D. A. *Acta Crystallogr.* **1995**, *D51*, 792.
(4) Hobom, G.; Braunitzer, G. *Z. Physiol. Chem.* **1967**, *348*, 783.
(5) Zimmermann, K.; Hagedorn, H.; Heuck, C. C.; Hinrichsen, M.; Ludwig, H. *J. Biol. Chem.* **1986**, *261*, 1653.
(6) Marvin, D. A.; Wiseman, R. L.; Wachtel, E. J. *J. Mol. Biol.* **1974**, *82*, 121.
(7) Marvin, D. A.; Pigram, W. J.; Wiseman, R. L.; Wachtel, E. J.; Marvin, F. J. *J. Mol. Biol.* **1974**, *88*, 581.
(8) Bhattacharjee, S.; Glucksman, M. J.; Makowski, L. *Biophys. J.* **1992**, *61*, 725.
(9) Miller, A.; Wray, J. S. *Nature* **1971**, *230*, 437.
(10) Smith, G. P.; Scott, J. K. *Methods Enzymol.* **1993**, *217*, 228.
(11) Nave, C.; Brown, R. S.; Fowler, A. G.; Ladner, J. E.; Marvin, D. A.; Provencher, S. W.; Tsugita, A.; Armstrong, J.; Perham, R. N. *J. Mol. Biol.* **1981**, *149*, 675.
(12) Symmons, M. F.; Welsh, L. C.; Nave, C.; Marvin, D. A.; Perham, R. N. *J. Mol. Biol.* **1995**, *245*, 86.
(13) Marvin, D. A.; Bryan, R. K.; Nave, C. *J. Mol. Biol.* **1987**, *193*, 315.
(14) Denny, R. C. *The CCP13 Newsletter No. 2*, Daresbury Laboratory: Warrington, U.K. 1993.
(15) Cochran, W.; Crick, F. H. C.; Vand, V. *Acta Crystallogr.* **1952**, *5*, 581.
(16) Klug, A.; Crick, F. H. C.; Wyckoff, H. W. *Acta Crystallogr.* **1958**, *11*, 199.
(17) Ramachandran, G. N. *Proc. Ind. Acad. Sci.* **1960**, *52A*, 240.
(18) Folkhard, W.; Marvin, D. A.; Watts, T. H.; Paranchych, W. *J. Mol. Biol.* **1981**, *149*, 79.
(19) Bernstein, F. C.; Koetzle, T. F.; Williams, G. J. B.; Meyer, E. F., Jr.; Brice, M. D.; Rodgers, J. R.; Kennard, O.; Shimanouchi, T.; Tasumi, M. *J. Mol. Biol.* **1977**, *112*, 535.
(20) Bunn, C. W.; Peiser, H. S.; Turner-Jones, A. *J. Sci. Inst.* **1944**, *21*, 10.
(21) Stroud, W. J.; Millane, R. P. *Acta Crystallogr.* **1995**, *A51*, 771.
(22) Stroud, W. J.; Millane, R. P. *Proc. R. Soc. London* **1996**, *A452*, 151.
(23) Tadokoro, H. *Structure of Crystalline Polymers*; Wiley: New York, 1979.
(24) Daubeny, R. de P.; Bunn, C. W.; Brown, C. J. *Proc. R. Soc. London* **1954**, *A226*, 531.
(25) Hall, I. H. In *Structure of Crystalline Polymers*; Hall, I. H., Eds.; Elsevier: London, 1984; p 39.
(26) Fraser, R. D. B.; MacRae, T. P.; Miller, A.; Suzuki, E. *J. Mol. Biol.* **1983**, *167*, 497.
(27) Wess, T. J.; Hammersley, A.; Wess, L.; Miller, A. *J. Mol. Biol.* **1995**, *248*, 487.
(28) Banner, D. W.; Nave, C.; Marvin, D. A. *Nature* **1981**, *289*, 814.
(29) Marvin, D. A.; Hohn, B. *Bacteriol. Rev.* **1969**, *33*, 172.
(30) Lapointe, J.; Marvin, D. A. *Mol. Cryst. Liq. Cryst.* **1973**, *19*, 269.
(31) Booy, F. P.; Fowler, A. G. *Int. J. Biol. Macromol.* **1985**, *7*, 327.
(32) Tang, J.; Fraden, S. *Liq. Cryst.* **1995**, *19*, 459.
(33) Gray, G. W.; Goodby, J. W. G. *Smectic Liquid Crystals*; Leonard Hill: Glasgow, 1984.
(34) Odijk, T. *Macromolecules* **1986**, *19*, 2313.
(35) Lekkerkerker, H. N. W.; Vroege, G. J. *Phil. Trans. R. Soc. London* **1993**, *A344*, 419.
(36) Day, L. A.; Marzec, C. J.; Reisberg, S. A.; Casadevall, A. *Annu. Rev. Biophys. Biophys. Chem.* **1988**, *17*, 509.
(37) Kramer, H.; Deggelmann, M.; Graf, C.; Hagenbüchle, M.; Johner, C.; Weber, R. *Macromolecules* **1992**, *25*, 4325.
(38) Kramer, H.; Graf, C.; Hagenbüchle, M.; Johner, C.; Martin, C.; Schwind, P.; Weber, R. *J. Phys. II Fr.* **1994**, *4*, 1061.
(39) Richards, F. M. *Methods Enzymol.* **1985**, *115*, 440.
(40) Nicholls, A.; Sharp, K. A.; Honig, B. H. *Proteins: Struct. Funct. Genet.* **1991**, *11*, 281.

MA9605614